Biochimica et Biophysica Acta 1828 (2013) 1802–1813

Contents lists available at SciVerse ScienceDirect

Biochimica et Biophysica Acta

journal homepage: www.elsevier.com/locate/bbamem

Mechanism of action of puroindoline derived tryptophan-rich antimicrobial peptides

Evan F. Haney [1], Alexandra P. Petersen, Cheryl K. Lau, Weiguo Jing, Douglas G. Storey, Hans J. Vogel *

Department of Biological Sciences, University of Calgary, Calgary, Alberta T2N 1N4, Canada

ARTICLE INFO

Article history:
Received 1 February 2013
Received in revised form 24 March 2013
Accepted 25 March 2013
Available online 2 April 2013

Keywords:
Antimicrobial peptide
Mechanism of action
NMR structure
Peptide–membrane interaction
Intracellular target

ABSTRACT

A tryptophan (Trp)-rich region in the wheat endosperm protein, puroindoline A, was previously shown to possess potent antimicrobial activity against Gram-positive and Gram-negative bacteria and this was attributed to the peptide inducing membrane instability. In the present work, the antimicrobial activity of the corresponding Trp-rich region in the puroindoline B isoform was examined and its antimicrobial activity was characterized. Unexpectedly, the puroindoline B Trp-rich peptide (PuroB) was relatively inactive compared to the related puroindoline A peptide (PuroA), despite strong sequence similarity. Using the sequence of PuroA as a template, a series of PuroB variants were synthesized and the antimicrobial activity was restored. Interestingly, all of these PuroB peptides preferentially interacted with negatively charged phospholipids, but unlike PuroA, they did not disrupt the integrity of lipid bilayers. This suggests that the primary mode of action of the PuroB peptides involves an antimicrobial target other than the bacterial membrane. Further tests revealed that all of the puroindoline derived peptides bind deoxyribonucleic acid (DNA) and block macromolecular synthesis *in vivo*. Based on these results, it appears that the interaction between puroindoline derived peptides and membranes is only an initial step in the mode of action and that binding to intracellular targets, such as DNA and ribonucleic acid (RNA), contributes significantly to their antimicrobial mode of action.

1. Introduction

The problem of antibiotic resistance has spurred continued interest in antimicrobial peptide research. Naturally occurring antimicrobial peptides continue to be discovered in a variety of organisms and *de novo* synthetic peptides have also been generated through combinatorial chemistry, for example [1]. A different approach to identifying antimicrobial peptides involves excising peptide fragments from larger proteins to generate novel sequences. This strategy has been used to identify a number of antimicrobial sequences including lactoferricin [2,3] and lactoferrampin [4], both antimicrobial peptides derived from the iron binding protein, lactoferrin. Other examples of antimicrobial peptides isolated from larger proteins include peptides derived from lysozyme [5] and histones [6,7]. In this study, we focus on a series of antimicrobial peptides based on sequences from wheat puroindolines.

Puroindolines are highly basic, Trp- and Cys-rich proteins found in wheat (*Triticum aestivum*) endosperm [8,9]. In fact, the name puroindoline is derived from *puros*, the Greek word for wheat, and the indole ring found in the side chain of Trp residues [10]. The pinA and pinB genes are both located in the hardness locus of the wheat genome and they encode the puroindoline A and puroindoline B proteins respectively [11,12]. These two puroindoline proteins share 55% sequence homology with each other and are unique because of the presence of 5 disulfide bonds, a large number of basic residues and a tryptophan-rich region [9]. In addition to controlling the hardness of the wheat kernels, puroindolines also exhibit antimicrobial and antifungal properties [13–16]. Part of this antimicrobial activity is thought to be related to the ability of full length puroindoline to induce pores in lipid bilayers [10,17], a feature which is attributed to the Trp-rich loop in the native protein. This is of particular interest because this region resembles other Trp-rich cathelicidin antimicrobial peptides such as bovine indolicidin [18] and porcine tritrpticin [19,20]. In an effort to understand the antimicrobial and lipid binding properties of the puroindolines, we sought to examine peptide fragments based on the Trp-rich loops from puroindoline A and B.

Our group previously studied a 13-residue peptide corresponding to the Trp-rich region in puroindoline A (FPVTWKWWKWWKG-NH_2).

Abbreviations: PuroA, puroindoline A derived peptide; PuroB, puroindoline B derived peptide; DSC, differential scanning calorimetry; ePC, Egg derived L-α-phosphatidylcholine; ePG, egg derived L-α-phosphatidylglycerol; DPPG, 1,2-dipalmitoyl-*sn*-glycero-3-phospho-(1′-*rac*-glycerol); DPPC, 1,2-dipalmitoyl-*sn*-glycero-3-phosphocholine; DiPoPE, 1,2-dipalmitoleoyl-*sn*-glycero-3-phosphoethanolamine; T_{hex}, hexagonal phase transition temperature; PLE, *E. coli* polar lipid extract; DPC, dodecylphosphocholine; diSC3-5, 3,3′-Dipropylthiadicarbocyanine iodide; Kd, dissociation constant; Ksv, Stern–Volmer constant; LUV, large unilamellar vesicle; MIC, minimum inhibitory concentration

* Corresponding author at: Department of Biological Sciences, University of Calgary, 2500 University Drive NW, Calgary, Alberta T2N 1N4, Canada. Tel.: +1 403 220 6006; fax: +1 403 289 9311.
E-mail addresses: evan@hancocklab.com (E.F. Haney), vogel@ucalgary.ca (H.J. Vogel).
[1] Present address: Center for Microbial Diseases and Immunity Research, Dr. R.E.W (Bob) Hancock Lab, University of British Columbia, Lower Mall Research Station, Room 257, 2259 Lower Mall UBC, Vancouver, BC, Canada, V6T 1Z4. Tel.: +1 604 822 9347.

0005-2736/$ – see front matter © 2013 Elsevier B.V. All rights reserved.
http://dx.doi.org/10.1016/j.bbamem.2013.03.023

This peptide exhibited potent antimicrobial activity against Gram-positive and Gram-negative bacteria and we concluded that this 13-mer (PuroA) constitutes the antimicrobial active center of puroindoline A [21]. The NMR structure of PuroA in the presence of SDS micelles adopts a partially helical amphipathic structure. In addition, PuroA preferentially interacts with negatively charged membranes and causes calcein leakage from negatively charged liposomes [21]. Based on these observations, it was concluded that PuroA employs a lytic mechanism to exert its antimicrobial effect.

The corresponding Trp-rich region in puroindoline B is a 12-mer (FPVTWPTKWWKG-NH_2) with remarkable sequence similarity to PuroA. However, when tested for antimicrobial activity, this 12-mer (PuroB1) was inactive compared to PuroA (see below). In this work, a series of peptides based on the PuroB1 sequence were synthesized in an attempt to increase the antimicrobial potency of this peptide. Three of these PuroB derivatives demonstrated antimicrobial activity against *Escherichia coli* and *Staphylococcus aureus* at similar concentrations to those seen for PuroA. Interestingly, biophysical characterization of the interactions between the PuroB peptides and lipids suggests that the principal mechanism of action does not involve the disruption of the bacterial membrane. Instead, our results suggest that the PuroB peptides cross the bacterial cytoplasmic membrane and bind to nucleic acids within the cell, blocking macromolecular synthesis of DNA, RNA and proteins. In addition, continued investigations of the PuroA peptide revealed that the membrane destabilizing effects of this peptide contribute to a more complex mode of action that also includes an intracellular mode of action.

2. Materials and methods

2.1. Chemicals and reagents

All the phospholipids (ePC, ePG, DPPG, DPPC, DiPoPE and PLE) as well as DPC were obtained from Avanti Polar Lipids (Alabaster, AL) as stock solutions dissolved in chloroform. SDS was obtained from EMD Chemicals Inc. (Gibbstown, NJ). 3,3′-Dipropylthiadicarbocyanine iodide (diSC3-5) was purchased from AnaSpec Inc. (Fremont, CA). Deuterated d_{25}-SDS was purchased from Cambridge Isotopes Laboratories (Andover, MA). [methyl-^{3}H]-thymidine (6.7 Ci/mmol) and [5-^{3}H]-uridine (25.5 Ci/mmol) were obtained from Perkin Elmer (Waltham, MA) while [ring-2,5-^{3}H]L-histidine (47.7 Ci/mmol) was purchased from Moravek Biochemicals and Radiochemicals (Brea, CA). All other reagents and chemicals were obtained from Sigma-Aldrich (St. Louis, MO).

2.2. Peptide sources

The puroindoline derived peptides were synthesized by AnaSpec (Fremont, CA) or at the University of Western Ontario peptide synthesis facility (London, Ont. Canada). All peptides were obtained at a purity of >95% as determined by HPLC and were used without further purification. The identity of each peptide was confirmed by mass spectrometry. All of the peptides were amidated at their C-terminus to remove the negative charge of the C-terminal carboxyl group. The sequences and net charges of the puroindoline peptides are shown in Table 1. Melittin (GIGAVLKVLTTGLPALISWIKRKRQQ-NH_2), purified from honey bee venom, was purchased from Sigma-Aldrich.

2.3. Peptide concentration determination

Peptide concentrations were determined based on the absorbance at 280 nm of a diluted peptide stock solution and the concentration was calculated according to Beer's law using theoretical extinction coefficients of 27500 M^{-1} cm^{-1}, 16500 M^{-1} cm^{-1} and 5500 M^{-1} cm^{-1} for PuroA, all the PuroB peptides and melittin respectively. Theoretical extinction coefficients were generated with the ProtParam tool on the ExPASY proteomics server [22].

Table 1
Sequences and net charges of the puroindoline peptides.

Peptide	Sequence	Net charge
PuroB1	FPVTWPTKWWKG-NH_2	+3
PuroB2	FPVTW**R**TKWWKG-NH_2	+4
PuroB3	F**R**VTW**R**TKWWKG-NH_2	+5
PuroB4	F**A**VTW**A**TKWWKG-NH_2	+3
PuroB5	F**K**VTW**K**TKWWKG-NH_2	+5
PuroA	FPVTWKWWKWWKG-NH_2	+4

2.4. Antimicrobial and hemolytic activity

The antimicrobial and hemolytic activities of the PuroB peptides were determined using the same procedure described for PuroA [21]. Briefly, *E. coli* ATCC 25922 and *S. aureus* ATCC 25923 were grown to the exponential phase in 2% Bacto Peptone water (Difco 1807-17-4). The cell suspensions were diluted to 2×10^6 cfu/ml (3.8×10^8 cfu/ml = 1U of A_{600}) in 2% Bacto Peptone Water and then added to the wells of 96-well polystyrene plates. Peptides were added to wells at concentrations ranging from 300 to 1.0 μg/ml and the plates were incubated overnight at 37 °C. The change in turbidity at 540 nm was measured and the MIC was defined as the lowest concentration of peptide that inhibited growth. All peptides were tested in triplicate.

To determine the hemolytic activity, human erythrocytes were isolated from heparinized human blood by centrifugation followed by three washes in phosphate-buffered saline (5 mM phosphate buffer, 150 mM NaCl, pH 7.4). Cell suspensions containing ~10^7 cells/ml were incubated with peptide for 30 min at 37 °C with gentle mixing. The cells were centrifuged and the absorbance at 540 nm was measured. Zero percent hemolysis was measured by adding phosphate buffer to the erythrocyte suspension while 100% hemolysis was achieved by adding 1% Triton X-100 to the erythrocytes.

2.5. Tryptophan emission fluorescence

Spectra were acquired on a Varian Cary Eclipse Fluorimeter (Varian Inc., Palo Alto, CA) equipped with a temperature control device set to 25 °C. Tryptophan emission spectra were collected between 300 and 450 nm using an excitation wavelength of 295 nm and excitation and emission slit widths of 10 nm. All samples contained 1 μM peptide in buffer (10 mM Tris, 150 mM NaCl. 1 mM EDTA, pH 7.4). Samples containing SDS and DPC were prepared to a final detergent concentration of 25 mM. Samples containing large unilamellar vesicles (LUVs, see calcein leakage section for details on LUV preparation) were made to a final lipid concentration of 30 μM.

Lipid binding was measured by titrating aliquots of *E. coli* polar lipid extract LUVs into 0.5 μM peptide solutions in buffer. After each addition of lipid, an emission spectrum was recorded between 300 and 400 nm using an excitation wavelength of 280 nm. Blank spectra were recorded for each addition of LUV into buffer and subtracted in the final analysis. The wavelength maxima (λmax) were determined by taking the slope of the emission spectra and using the wavelength where this value was closest to zero. The λmax values were plotted as a function of lipid concentration and the dissociation constants (Kd) were calculated in CaLigator [23] using a least-squares fit algorithm and a one-site binding model. The CaLigator software is typically used to determine calcium binding constants to proteins but it can also be used to evaluate the binding of any two interacting partners.

2.6. Acrylamide quenching of emission fluorescence

Stern–Volmer constants (Ksv) [24] were calculated as described previously [25,26]. Briefly, 5 μl aliquots of a 4 M acrylamide solution

were added to the fluorescence samples containing 1 μM peptide described above. After each addition of acrylamide, a tryptophan emission spectrum was acquired. The Ksv for each combination of peptide and lipid was calculated using the following formula:

$$F_o/F = 1 + K_{sv}[Q]$$

where F_o is the maximum fluorescence emission intensity of the peptide in buffer and F is the intensity following the addition of the soluble quencher, Q.

2.7. Differential scanning calorimetry

DSC experiments with DPPG and DPPC phospholipids were performed according to a modified protocol originally described by Prenner et al. [27]. DiPoPE experiments were carried out according to Powers et al. [28]. Briefly, 0.5 mg of DPPG, 0.5 mg of DPPC lipid or 5 mg of DiPoPE from stock chloroform solutions was added to small glass vials and lipid films were generated as described above. To prepare the DSC sample, the lipid film and buffer (20 mM sodium phosphate with 130 mM NaCl, pH 7.4 for DPPG and DPPC samples or 10 mM Tris, 100 mM NaCl, 2 mM EDTA pH 7.4 for DiPoPE samples) were heated for 15 min at 55 °C and then warm buffer was added to the lipid and vortexed vigorously. The DiPoPE samples were also sonicated for ~3 h to resuspend the lipid. Following lipid resuspension, peptide was added from a stock solution to give a final lipid:pepide molar ratio of 10:1. Samples of pure lipid were also prepared for comparison. The final lipid concentration in the DPPC and DPPG samples was 0.5 mg/ml while the DiPoPE samples were all prepared to a final lipid concentration of 5 mg/ml. All DSC experiments were carried out on a Microcal high-sensitivity VP-DSC instrument (Microcal, Northampton, MA). For the DPPG and DPPC samples, an initial buffer–buffer scan between 20 and 60 °C was performed then the degassed lipid and peptide mixture was loaded into the sample cell as it cooled. Four heating scans were performed between 20 and 60 °C at a scan rate of 10 °C/h. For the DiPoPE samples, five heating scans were recorded between 10 and 60 °C at a scan rate of 60 °C. In all cases, the final heating scan was analyzed in the Microcal Origin software package (version 7.0).

2.8. Circular dichroism spectroscopy

CD spectra were acquired at room temperature on a Jasco-J810 Spectropolarimeter (Jasco, Easton, MD) using a 1 mm pathlength cuvette. Each sample contained 50 μM peptide in buffer (25 mM sodium phosphate buffer, pH 7) or in a buffered solution with 30 mM SDS. A blank spectrum, lacking peptide, was also recorded and subtracted in the final analysis. Far-UV CD spectra were collected between 260 nm and 190 nm using a 0.5 nm step size and a scanning speed of 100 nm/min. The bandwidth was set to 1 nm and the response was set to 0.5 s. Ten spectra were accumulated and averaged to generate the final spectra. The mean residue ellipticity was calculated according to Wallace and Janes [29].

2.9. NMR structure determination

NMR structure determination was performed on unlabelled peptide samples using two-dimensional NMR spectroscopy. Samples were prepared by dissolving the lyophilized peptide in a 90:10 mixture of H_2O:D_2O to a final concentration of 1–2 mM. DSS was added as an internal standard to a final concentration of 20 μM and the pH was adjusted to between 3.5 and 4.5 using HCl or NaOH. Following data collection on the aqueous sample, deuterated SDS (Cambridge Isotopes Laboratories, Inc. Andover, MA) was added to a final concentration of 200 mM and the pH was readjusted to fall within the same range.

All NMR spectra were recorded on a Bruker Avance 700 MHz spectrometer at 298°K. Two-dimensional NOESY spectra were recorded for the aqueous peptide samples using a mixing time of 500 ms. NOESY, TOCSY and COSY spectra were acquired for the detergent containing samples. Mixing times of 100 ms and 120 ms were used in these NOESY and TOCSY experiments respectively. Data were collected with 4096 × 600 data points in the F2 and F1 dimensions at a sweep width of 8992.806. Water suppression was achieved using excitation sculpting [30]. Processing of the spectra was performed using the NMR pipe software [31]. The 2-D data were zero filled once in each dimension and Fourier transformed with a shifted sine-bell function. Visualization and analysis of all the spectra was performed in NMRView [32].

Starting structures for the PuroB peptides were generated with CNS [33] and the micelle bound peptide structures were calculated using the simulated annealing protocol in ARIA 1.2 [34]. Peptide structures were calculated based on NOE crosspeaks assigned from the 2D ^{1}H-NOESY spectra. The backbone *phi* and *psi* angles of non-Gly and Pro residues were also restrained to fall within allowed regions of the Ramachandran plot [35]. Nine iterations of simulated annealing were performed with 20 structures calculated in the first 7 iterations followed by 40 and 100 structures in the final two iterations respectively. The 20 lowest energy structures from the final iteration were used in the final analysis. The 3-D peptide structures were visualized in MOLMOL [36] and the quality of the structures was evaluated with Procheck [37].

2.10. Calcein leakage from LUVs

The release of calcein from LUVs of varying composition was measured for all five PuroB derivatives using the procedure described by Nguyen et al. [38]. Melittin, a known lytic peptide, was used as a positive leakage control. Lipid films were prepared by placing 1 mg of stock lipid solution, dissolved in chloroform, in a glass vial. The chloroform was evaporated in a stream of nitrogen gas and the resulting lipid film was placed under vacuum for ~2 h to remove any trace organic solvent. Lipid films were kept at −20 °C until ready for use. To generate calcein encapsulated LUVs, lipid films were resuspended in buffer (10 mM Tris, 150 mM NaCl, 1 mM EDTA, pH 7.4) containing 70 mM calcein. Calcein free LUVs, used in the tryptophan fluorescence experiments, were generated in the same way using calcein free buffer. The lipid suspension was subjected to 5 cycles of liquid nitrogen freezing and warm water thawing followed by 15 passes through two 0.1 μM polycarbonate filters using a mini-extruder apparatus (Avanti Polar Lipids, Alabaster). The calcein encapsulated LUVs were separated from free calcein as the first strong yellow fraction to elute from a Sephadex G50 gel filtration column. The lipid concentration in each LUV preparation was determined by measuring the phosphate concentration according to the procedure developed by Ames [39]. The lipid composition of the LUVs tested for calcein leakge was: DPPC, DPPC:DPPG, ePC, ePC:ePG and *E. coli* polar lipid extract (PLE).

2.11. E. coli cytoplasmic membrane depolarization

Membrane depolarization of *E. coli* was measured using a modified protocol originally described by Chongsiriwatana and Barron [40]. The antibiotic-susceptible DC2 *E. coli* strain [41] was obtained from the CGSC (Yale University, New Haven, CT) and was used in these experiments because it possesses a defective outer membrane, giving the peptide access to the bacterial cytoplasmic membrane without the need for EDTA [42]. Bacterial cultures in LB broth were grown at 37 °C to an OD_{600} of ~0.4 and then 5 ml of culture was harvested at ~3200 ×*g* for 10 min. The cell pellet was resuspended in 5 ml of respiration buffer (5 mM HEPES, 20 mM glucose, pH 7.4) and then 10–20 ml of an OD_{600} of 0.05 DC2 cell suspension was prepared and kept at 4 °C until the addition of diSC3-5. 1 h prior to measuring the membrane depolarization, diSC3-5 was added to 1.5 ml of

the DC2 cell suspension to a final concentration of 0.2 μM. This aliquot was equilibrated at room temperature for 1 h, with occasional mixing. 1 ml was transferred to a quartz cuvette and the fluorescence emission intensity at 670 nm (excitation 622 nm) was measured for 1 min. The peptide was then added to a final concentration of 6 μM and the fluorescence was measured for 5 min. Finally, 10 μl of a 10% Triton-X100 solution was added and the fluorescence intensity was monitored for an additional 9 min. As a positive control, the membrane depolarization induced by 20 μM melittin was measured as indicated by Chongsiriwatana and Barron [40].

2.12. DNA binding assay

To examine peptide binding to DNA, an agarose gel-retardation assay was performed similar to that described by Park et al. [43]. Unmodified pET-19b plasmid was purified from an overnight 5 ml culture of DH5α cells harboring the vector using the Qiagen Plasmid Purification Kit (Qiagen Inc.Valencia, CA). The purified plasmid concentration was determined using a NanoDrop instrument (NanoDrop Products, Wilmington, DE). 100 ng of the plasmid was incubated at room temperature with increasing amounts of peptide in 20 μl of binding buffer (5% glycerol, 10 mM Tris–HCl at pH 8.0, 1 mM EDTA, 1 mM DTT, 20 mM KCl and 50 ug/ml BSA). After 1 h of incubation, 4 μl native loading buffer (10% Ficoll 400, 10 mM Tris–HCl, 50 mM EDTA, 0.25% bromophenol blue at pH 7.5) was added to the mixture. 12 μl of this solution was loaded onto a 1% agarose gel in Tris-acetate-EDTA (TAE) buffer containing ethidium bromide for visualization of the DNA bands. The gel was run at 100 V for 30 min and imaged on a Bio-Rad Geldoc XR (Bio-Rad Laboratories, Hercules CA).

To determine the binding affinity of the puroindoline peptides to pET-19b plasmid DNA, the density of the plasmid bands in the agarose gels was determined with the Bio-Rad Quantity One imaging software package. The resulting band intensities were plotted as a function of deoxyribonucleotide concentration and the Kd values were calculated with CaLigator in the same manner as the lipid binding experiments.

2.13. Macromolecular synthesis inhibition

The inhibition of DNA, RNA and protein synthesis in *E. coli* was determined using the procedure described by Patrzykat et al. [44]. *E. coli* CGSC 4908 (auxotrophic for thymidine, uridine and L-histidine) was obtained from the CGSC at Yale University (New Haven, CT).

Overnight cultures of CGSC 4908 were grown in LB broth starting from a single colony selected from a fresh LB-agar streak plate. The following day, 10 μl of the overnight culture was added to 10 ml of LB broth and grown to the exponential phase (OD 600 nm of ~0.3). The cells were harvested at 3220 ×*g* for 5 min at 4 °C and then resuspended in an equal volume of M9 minimal media [45]. 300 μl aliquots of resuspended cells were supplemented with 9 μl of either [^{3}H]thymidine, [^{3}H]uridine or [^{3}H]L-histidine and 100 mg/l of the other two unlabeled precursors. The cultures were incubated for 5 min at 37 °C, at which point 3 μl of stock peptide solution was added to achieve final peptide concentrations of 3, 6, 30 or 60 μM. 50 μl of the bacterial culture was removed prior to the addition of peptide (time = 0) and added to 5 ml of ice cold 10% trichloroacetic acid (TCA) containing 200 mg/l of unlabeled precursors. This process was repeated at time points of 5, 15 and 30 min. After 40 min on ice, the TCA samples were transferred to a 37 °C water bath and incubated for 15 min. DNA, RNA and protein were collected over vacuum using 25 mm nucleic acid and protein transfer filters from Whatman GmbH (Dassel, Germany). The filters were rinsed 10 times with ice cold 10% TCA and dried in an oven at 70 °C. Each filter was placed in a scintillation vial with 20 ml of BCS-NA non-aqueous biodegradable counting scintillant (GE Healthcare) and radioactive counts for each sample were recorded for 1 min using a Beckman LS6500 multi-purpose scintillation counter (Beckman Coulter, Brea, CA.).

Growth assays for CGSC 4908 were performed as described above using M9 minimal media supplemented with 100 mg/l of unlabeled precursors. At each time point, a 5 μl aliquot of the bacterial cell suspension was diluted 40,000× and 100 μl of this dilution was spread onto LB-agar plates. The plates were incubated overnight at 37 °C and cfus were counted the following day.

3. Results

3.1. Antimicrobial and hemolytic activity

MICs for the PuroB peptides against *E. coli* and *S. aureus* are shown in Table 2. PuroB1, which directly corresponds to the Trp-rich region in puroindoline B, is relatively inactive. PuroB4, in which the two proline residues of PuroB1 have been replaced by Ala, is also inactive under the conditions tested. PuroB2, PuroB3 and PuroB5 have mutations to the Pro residues which introduce basic Arg and Lys residues to the peptide sequence. All three of these peptides exhibit significant antimicrobial activity, with MIC values comparable to that determined for PuroA. Given that hemolysis of red blood cells only occurred at peptide concentrations exceeding 300 μM, the PuroB peptides are considered to have weak cytotoxic activity.

3.2. Tryptophan emission fluorescence

Tryptophan emission fluorescence of the PuroB peptides in a variety of membrane mimetics was performed to examine the environment surrounding the Trp residues when the peptides interact with membranes. A blue shift in the maximum emission wavelength occurs when a Trp residue moves into a more hydrophobic environment and is typically interpreted as the indole moiety inserting into the hydrophobic core of a bilayer. In buffer, all of the peptides had a Trp emission maximum at ~357 nm (Table 3). When SDS or DPC micelles were added to the peptides, a significant blue shift was observed. Strong blue shifts were also seen when negatively charged LUVs were added, suggesting that an electrostatic attraction between the anionic lipids and the cationic residues is important for lipid binding. When mixed with ePC LUVs, none of the peptides demonstrated any significant blue shift, further implicating the negative charge as an essential component of the peptide-lipid interactions. The blue shifts seen with the zwitterionic detergent DPC are likely due to the detergent bound conformation of the PuroB peptides being favoured because of the high concentration of detergent used in the fluorescence experiments as opposed to an electrostatic attraction with the micelle surface.

3.3. Tryptophan fluorescence quenching

The quenching of Trp emission fluorescence by the soluble acrylamide quencher provides information about the accessibility of the Trp fluorophores when the peptide is bound to a membrane. If a peptide binds to the surface of a membrane and the Trp residues insert into the hydrophobic core of the bilayer, then they are no longer

Table 2
Antimicrobial and hemolytic activity of puroindoline derived peptides.

Peptide	MIC *E. coli* (μM)	MIC *S. aureus* (μM)	Hemolytic concentration (μM) EC_{50}
PuroB1	>125	>125	>300
PuroB2	15.5	>3.1	>300
PuroB3	6.0	<3.0	>600
PuroB4	>125	100	>300
PuroB5	3.1–6.2	6.2–9.3	>600
PuroA[a]	5.3	20	>500

[a] Previously published by Jing et al. [21].

Table 3
Blue shifts (in nm) of the fluorescence emission maximum wavelength for the PuroB peptides in various lipid environments. Values are indicated relative to the wavelength of the maximum emission fluorescence of each peptide in buffer (Buffer max λ). The concentration of SDS and DPC in these experiments was 25 mM while the phospholipid concentration in the LUV containing samples was 30 μM.

Peptide	Buffer max λ	Micelles		LUVs			
		SDS	DPC	ePE:ePG	3:1 ePE:ePG	ePC:ePG	ePC
PuroB1	358	16	13	11	3	12	−1
PuroB2	357	13	11	6	2	9	2
PuroB3	357	13	8	9	5	10	0
PuroB4	357	12	13	10	2	13	0
PuroB5	357	13	9	12	7	10	0

accessible to the effects of the soluble quencher. Therefore, a low Ksv indicates that the fluorophore is buried into the hydrophobic core of a bilayer. The relative Ksv values for the PuroB peptides are shown in Fig. 1. All of the Ksv results are shown as relative values compared to the Ksv of the peptide in buffer, which has been assigned a value of 1. Consistent with the blue shift results, all of the PuroB peptides had similar relative Ksv values under the conditions tested. All of the micelle bound peptides produced relative Ksv values roughly 50% lower than the values determined in buffer. When tested with LUVs, all of the peptides displayed lower Ksv values compared to buffer, but the decrease in relative Ksv was directly related to the net negative charge on the surface of the vesicle. In LUVs where half of the head groups were PG, there was a reduction in the K_{sv} values of roughly 40%. This decrease was not as pronounced when the peptides were mixed with 3:1 ePE:ePG LUVs, wherein the lower concentration of ePG results in fewer negative charges on the surface of the vesicles. When mixed with zwitterionic ePC LUVs, the PuroB peptides had K_{sv} values that were approximately 80% of the Ksv reported in buffer. This is likely due to a weaker interaction between the peptides and the charge neutral vesicles.

Based on the fluorescence results, the PuroB derived peptides preferentially interact with negatively charged lipid species. However, all of the peptides appear to interact with bilayers in a similar fashion and there are no significant differences between the peptides to explain the variation in the MIC values.

3.4. Differential scanning calorimetry

The influence of the PuroB peptides on the thermotrophic phase behavior of DPPC and DPPG lipid suspensions was examined with DSC. The zwitterionic PC head group is used as a mimic for eukaryotic membranes while the negatively charged PG head group is representative of bacterial membranes [46]. None of the PuroB peptides caused significant changes in the DSC thermograms of DPPC lipids at peptide:lipid ratios of 1:10. The main phase transition of pure DPPC occurs at ~41 °C and it was relatively unaffected by the addition of any of the PuroB peptides (Fig. 2).

The addition of the PuroB peptides to DPPG lipid suspensions had a much stronger effect on the thermotrophic phase behaviour of the anionic phospholipids (Fig. 3). Pure DPPG lipids showed a pre-transition at ~33 °C and a main phase transition at ~40 °C. The addition of PuroB1 and PuroB4 to DPPG lipids caused the pre-transition to disappear and the main phase transition broadened slightly and shifted to a lower temperature of ~38 °C. The addition of PuroB2 had a similar effect, except that there appears to be two peaks comprising the main phase transition at 38 °C. This suggests that these peptides insert into the hydrophobic core of DPPG bilayers and destabilize the phase transition between the lamellar gel phase and the liquid crystalline phase.

The addition of PuroB3 and PuroB5 to DPPG lipid suspensions resulted in the largest changes in the DSC thermograms compared to the pure lipid. When mixed with PuroB3, the heating scan showed a main phase transition centered at ~38 °C and a small peak at ~43.5 °C. When PuroB5 was added, it virtually abolished the main phase transition peak and a high temperature transition at ~56 °C appeared. The higher temperature transitions in the presence of PuroB3 and PuroB5 suggest the formation of stable lipid–peptide complexes that behave differently compared to pure DPPG or any of the other peptides. Evidently the cationic residues at position two in PuroB3 and PuroB5 do not impede membrane insertion of the N-terminal region of the peptides. Instead, it appears that this added positive charge causes significant changes in bilayer organization. In general, the DSC results demonstrate that the PuroB peptides interact with negatively charged phospholipids and all of them insert into the acyl chains of the bilayer.

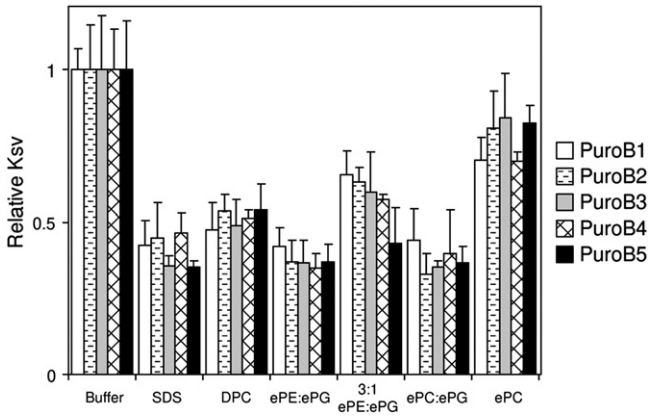

Fig. 1. Relative Ksv values calculated for the PuroB peptides in various lipid environments. The average Ksvs of the peptide determined in buffer was arbitrarily assigned a value of 1 and the error bars represent the standard deviation of three separate trials. The concentration of SDS and DPC in these experiments was 25 mM while the phospholipid concentration in the LUV containing samples was 30 μM.

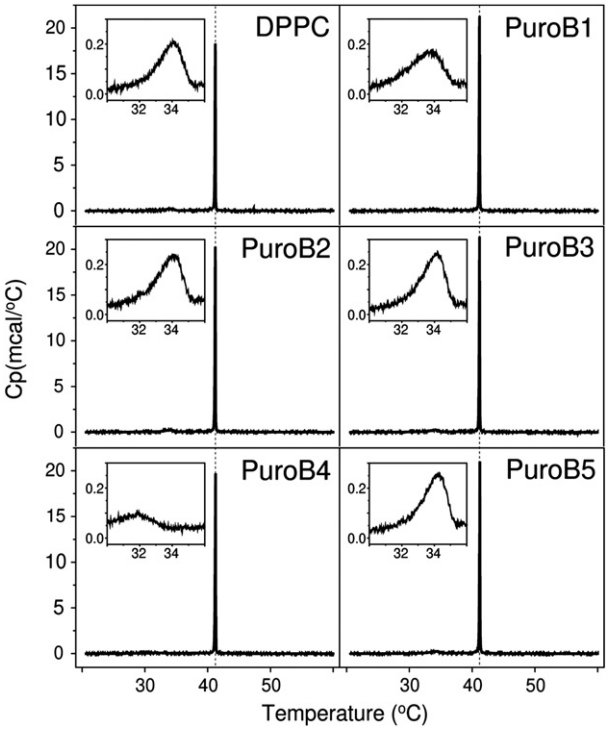

Fig. 2. Differential scanning calorimetry thermograms of a 0.5 mg/ml DPPC lipid suspension and DPPC mixed with the PuroB peptides added at a lipid:peptide ratio of 10:1. The insets show a magnification of the pretransition region of the DSC scan and the vertical dashed line at ~41 °C corresponds to the main phase transition temperature (T_m) of the lamellar gel phase to the liquid crystalline phase of pure DPPC.

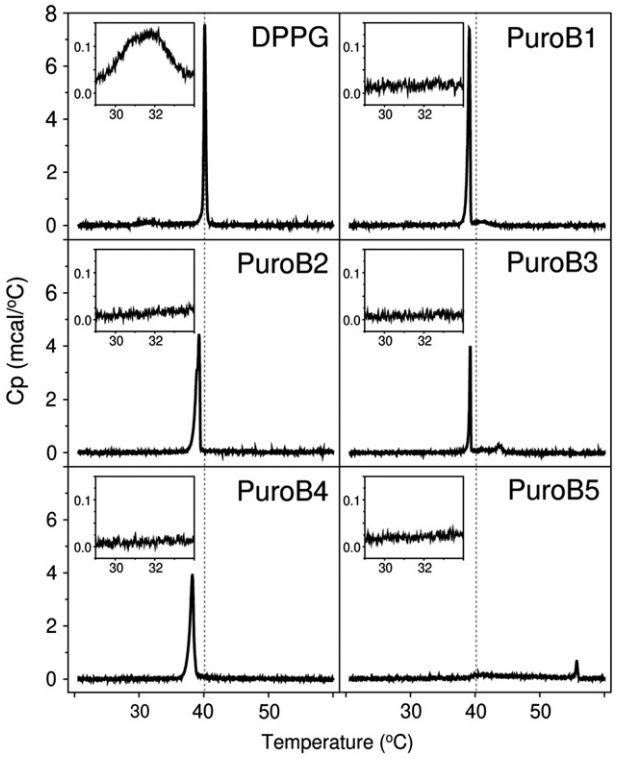

Fig. 3. DSC thermograms of 0.5 mg/ml DPPG lipid compared to DPPG mixed with the PuroB peptides at a final lipid:peptide ratio of 10:1. The vertical dashed line at ~40 °C corresponds to the T_m of pure DPPG.

DiPoPE lipids are often used to measure the ability of a peptide to induce membrane curvature by monitoring the shift in the liquid crystalline (L_α) to inverted hexagonal phase transition (H_{II}) [47,48]. The effect of the PuroB peptides on the hexagonal phase transition temperature (T_{hex}) of DiPoPE lipids was evaluated using DSC (Fig. 4). Usually, an increase in the T_{hex} is consistent with an induction of positive membrane curvature which is often associated with the formation of pores in a bilayer [49]. Interestingly, while all of the PuroB peptides shifted the T_{hex} to a higher temperature, none of the PuroB peptide significantly destabilized model membranes or *E. coli* cytoplasmic membranes (see calcein leakage and membrane depolarization results below). Therefore, another interpretation of the observed increase in the T_{hex} by the PuroB peptides is that these peptides stabilize the lamellar phase of DiPoPE lipids. This would inhibit the formation of the inverse hexagonal lipid phase and shift the T_{hex} to a higher temperature but would also explain why the peptides do not destabilize the integrity of bilayers. To the best of our knowledge, this is the first example of a peptide that increases the T_{hex} of DiPoPE lipids but does not induce pores in phospholipid bilayers.

3.5. Circular dichroism spectroscopy

Circular dichroism spectra of the puroindoline peptides were recorded in buffer and in the presence of SDS micelles (Fig. 5). In buffer, all of the puroindoline B peptides had strong negative peaks at ~200 nm, indicative of unstructured peptides. There is also a strong peak at ~223 nm in all the spectra which is likely due to interactions between neighbouring Trp residues in the peptides [50]. When SDS micelles were added to the samples, all of the PuroB peptides underwent a conformational change, as seen by the emergence of a new minima peak at ~226 nm. In addition, all of the PuroB peptides, except PuroB4, saw another positive peak appear at ~215 nm. For PuroB4, an increase in the mean residue ellipticity (MRE) values

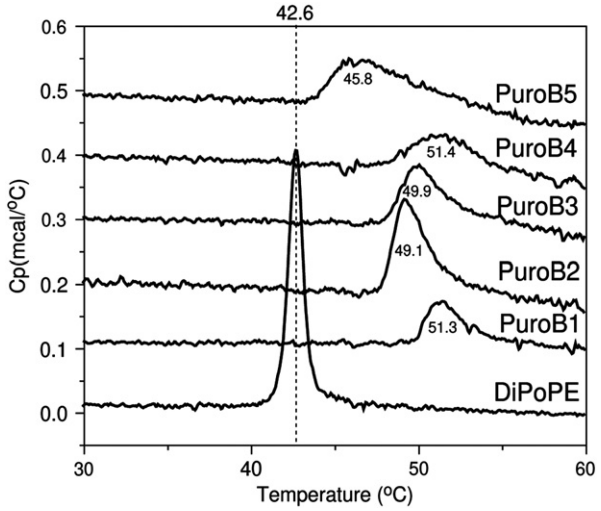

Fig. 4. Influence of the PuroB peptides on the liquid crystalline to inverted hexagonal phase transition temperature (T_{hex}) of DiPoPE lipids. A DSC scan of pure DiPoPE is shown for comparison. The T_{hex} of pure DiPoPE is 42.6 °C and the transition temperatures for the peptide containing samples are indicated. The concentration of lipid in each sample was 5 mg/ml and a molar lipid:peptide ratio of 10:1 was used.

near 195 nm was observed. Additionally, the CD spectrum of PuroB1 in SDS retains a relatively strong minima at 200 nm which could be due to the presence of multiple peptide conformations within the sample (see NMR structure section below).

Overall, the CD spectral features of the PuroB peptides bound to SDS micelles are not characteristic of any type of regular secondary structure element (ie. α-helix or β-sheet) but the increase in MRE at 210 nm might be due to the presence of β-turn conformations

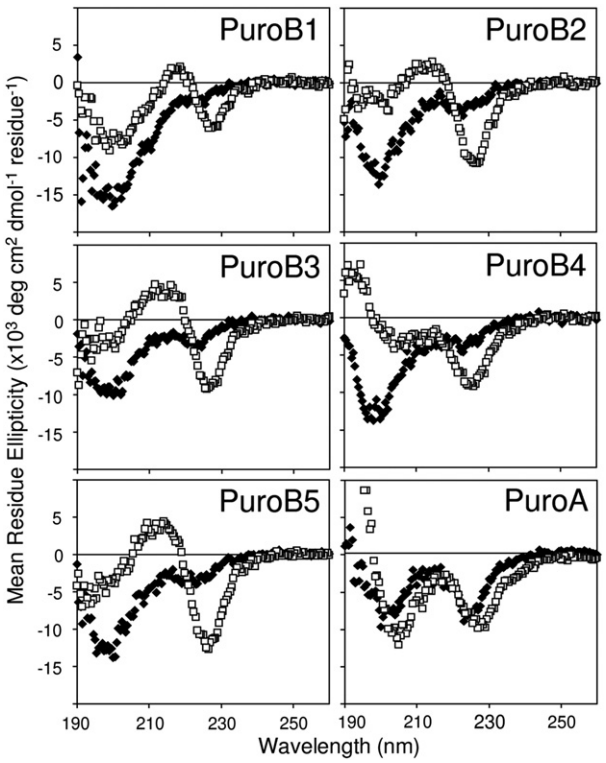

Fig. 5. Circular dichroism spectra of the puroindoline derived peptides in buffer (♦) and in the presence of 30 mM SDS (□). All spectra were recorded at a peptide concentration of 50 μM at room temperature.

[51]. Since all of the CD spectra of the PuroB peptides are comparable to each other, we can conclude that they all adopt similar SDS bound conformations that are different from their structures in aqueous solution. In contrast, the CD spectrum of PuroA in the presence of SDS micelles is remarkably similar to that observed in buffer (Fig. 5), suggesting that PuroA does not undergo a large conformational change when it binds to membranes.

3.6. Micelle bound NMR solution structures of PuroB peptides

Consistent with the CD results, all of the PuroB peptides appeared to be unstructured in aqueous solution based on the lack of cross peaks in the NOESY spectra (data not shown). Upon the addition of deuterated SDS micelles, the PuroB peptides underwent a conformational change to a micelle bound state. The NOESY spectra of PuroB2, B3, B4 and B5 in the presence of SDS were all well resolved with excellent peak separation. In the case of PuroB1, the presence of the two Pro residues significantly complicated the NMR structural analysis. It appears that *cis-trans* isomerisation across these two Pro residues yielded multiple conformations for micelle bound PuroB1 (see Supplementary Fig. 1). Considering that PuroB1 displayed poor antimicrobial activity (Table 2) and that the conformation was similar to the other puroindoline B derived peptides (see CD spectroscopy results), the NMR structure of micelle bound PuroB1 was not pursued further.

The solution structures of the remaining PuroB peptides bound to SDS micelles are shown in Fig. 6. Structural statistics for resulting structures are shown in Supplementary Table 1. All four peptides adopt extended conformations with well defined backbone RMSDs ranging from ~0.3 to 0.6 Å when the structures are superimposed across residues 2–11. The structures of the PuroB peptides bound to SDS micelles are largely amphipathic with Phe1, Val3 and the three Trp residues forming a large hydrophobic surface on one face of the peptide, while the cationic and hydrophilic residues (Arg, Lys and Thr) appear on the opposite face. The exception to this is the positively charged Arg6 in PuroB3 which is oriented directly in the middle of the hydrophobic face of the peptide. Upon closer inspection, the indole ring of Trp5 is parallel to the Arg side chain, suggesting that there could be a cation–pi interaction between these two residues (*e.g.* see Chan et al. [52]). This interaction likely shields some of the positive charge of the guanidinium group from the negatively charged micelles while still allowing for the peptide to interact with membranes.

The solution structures of the PuroB peptides shown here suggest a binding model wherein the peptide inserts at the interfacial region of a negatively charged membrane. Based on this structure, the hydrophobic residues penetrate into the hydrophobic core of the membrane while the positive charges interact with the negative charges of the lipid head groups.

3.7. Calcein leakage

The PuroB peptides as well as PuroA were examined for their ability to induce leakage of the self quenching dye, calcein, from LUVs of varying composition. Melittin, a peptide with known membrane destabilizing activity, was used as a positive control for membrane leakage. Interestingly, the percent of calcein leakage induced by the PuroB peptides was comparable to the intrinsic leakage of the LUVs over the course of the experiment, suggesting that the PuroB peptides do not disrupt the integrity of phospholipid bilayers under the conditions tested (Fig. 7A). PuroA caused significant leakage from LUVs composed of DPPC:DPPG, ePC or ePC:ePG while very little calcein release was observed from vesicles composed of DPPC or PLE. This suggests that the membrane perturbing properties of PuroA are dependent on the type of phospholipid that makes up the vesicles.

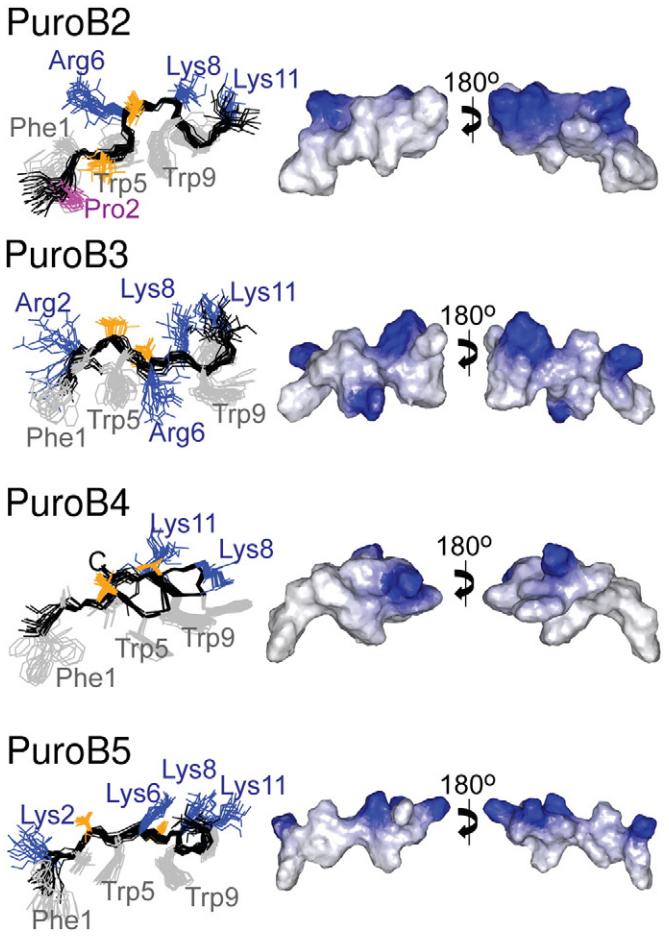

Fig. 6. NMR solution structures of PuroB2, PuroB3, PuroB4 and PuroB5 bound to SDS micelles. The panel on the left highlights specific residues with hydrophobic residues shown in grey, Thr indicated in orange and positively charged residues coloured blue. The panel on the right depicts the surface charge distribution of the PuroB peptides with positively charged regions shown in blue.

3.8. Membrane depolarization of E.coli DC2

The capacity of the puroindoline derived peptides to depolarize the cytoplasmic membrane of *E. coli* DC2 cells was examined and compared to the depolarization caused by the lytic peptide, melittin. All of the PuroB peptides as well as PuroA caused significantly less depolarization of the bacterial cytoplasmic membrane compared to melittin (Fig. 7B). While it is unknown what amount of membrane depolarization correlates with the determined MICs, it is evident that the puroindoline peptides do not depolarize the bacterial cytoplasmic membrane to the same extent as melittin.

3.9. DNA binding by inhibition of plasmid migration in an agarose gel

DNA binding by the PuroB peptides was indirectly measured by monitoring the effect of increasing peptide concentration on the migration of purified pET-19b plasmid DNA in a 1 % agarose gel (Fig. 8). PuroB1 demonstrated the weakest ability to inhibit plasmid migration since strong DNA bands were still observed at peptide: plasmid weight ratios as high as 30:1. PuroB4 had the next lowest capacity to inhibit plasmid DNA migration with strong plasmid bands still present at ratios as high as 10:1 with weaker bands observed at 20:1 and 30:1 as well. PuroB2, PuroB3 and PuroB5 all had stronger DNA binding affinities compared to PuroB1 and PuroB4. PuroB2 showed significant inhibition of DNA migration at peptide:DNA ratios higher than 10:1, PuroB3 stopped DNA migration at a ratio of 5:1 and PuroB5 inhibited DNA migration at a weight ratio of 1:1, the strongest

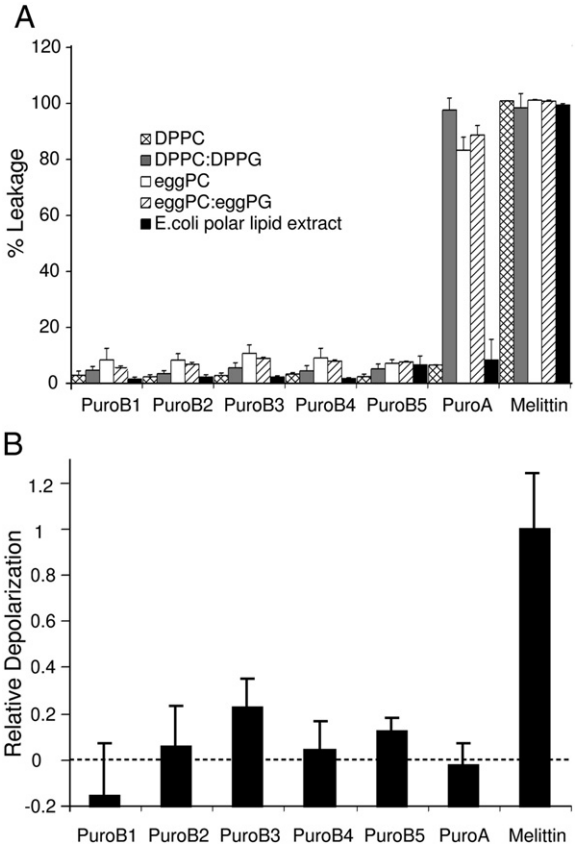

Fig. 7. Membrane perturbation caused by the puroindoline derived peptides. (A) Percentage of calcein dye release from LUVs by the PuroB peptides, PuroA and melittin. Peptides were added to achieve a final lipid:peptide molar ratio of 10:1. The lipid composition for each LUV is indicated and error bars represent the standard deviation of three separate trials. (B) Percent membrane depolarization of *E. coli* DC-2 cells induced by the PuroB peptides and PuroA at a concentration of 6 μM. The membrane depolarization induced by 20 μM melittin has been assigned a maximal depolarization value of 100%. Error bars represent the standard deviation of four separate trials.

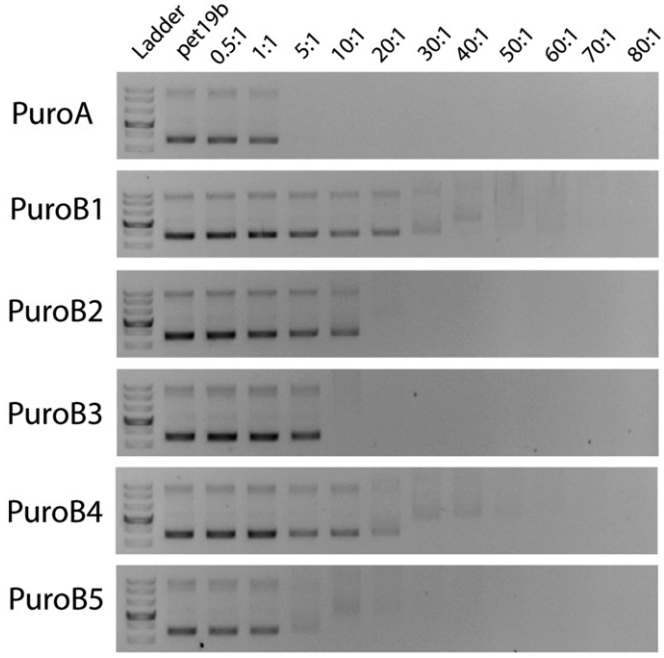

Fig. 8. Inhibition of pET-19b plasmid migration in a 1% agarose gel by the puroindoline peptides. Peptide and plasmid were incubated at room temperature for 1 h at increasing peptide:plasmid weight ratios, indicated at the top of each lane. Pure pET-19b plasmid was also run as a negative control in lane 2.

of all the puroindoline B derived peptides. Interestingly, PuroA also exhibited a strong capacity to bind to plasmid DNA as pET-19b bands could not be seen at weight ratios above 1:1.

3.10. Dissociation constants for peptide binding to DNA and phospholipids

The dissociation constants (Kds) calculated for the puroindoline derived peptides binding to pET-19b plasmid DNA or *E. coli* polar lipid extract LUVs are shown in Table 4. The DNA binding Kds are reported per deoxyribonucleotide base while the lipid binding Kds are per phospholipid. For an example and complete description of the calculations used to determine the Kds for DNA and *E. coli* polar lipid binding, see Supplementary Fig. S2. All of the lipid binding affinities were similar for all of the PuroB peptides with values ranging from ~20 to 40 μM, representing relatively weak lipid binding. The dissociation constants determined for the PuroB peptides binding to DNA were more varied. The strongest binding peptides were PuroB2, PuroB3 and PuroB5 with average Kd values between 2 and 10 μM. This is 5–20 times stronger than the affinities determined for lipid binding. Conversely, PuroB1 and PuroB4 bound deoxyribonucleotides weakly. The Kd values determined for PuroA binding to both DNA and lipids were the strongest of all the peptides tested.

A comparison between the two calculated Kd values gives an indication as to which biomolecule the puroindoline peptides preferentially bind. In the case of PuroB1 and PuroB4, the Kds for DNA and lipid binding are roughly equivalent (within error) which demonstrates that there is no preference for binding. For all the other peptides, their affinities for DNA were 2 to 10 times stronger, suggesting that it is more favorable for these peptides to bind to DNA than membranes.

3.11. Macromolecular synthesis inhibition

E. coli CGSC 4908 is a bacterial strain auxotrophic for thymidine, uridine and L-histidine [53]. The incorporation of radioactive versions of these precursors into DNA, RNA and protein was monitored over time in the presence of the puroindoline derived peptides and compared to cultures grown in the absence of peptide. Control experiments were performed with ciprofloxacin, rifampin and chloramphenicol as inhibitors of DNA, RNA and protein synthesis respectively (See Supplementary Fig. S3).

Based on the MIC values determined for *E. coli* in Table 2, peptide concentrations of 3, 6, 30 and 60 μM were examined for their ability to kill *E. coli* CGSC 4908 over the course of the 30 min incubation. These concentrations were chosen because they cover all of the MIC values for the most active peptides that were tested with the tritiated compounds. The effects of PuroB1 and PuroB4 on macromolecular synthesis in *E. coli* CGSC 4908 were not determined because these two peptides were inactive in this concentration range.

Of the peptides tested in this study, PuroA was the most potent against *E. coli* ATCC 25922 (Table 2). When examined against CGSC 4908, PuroA caused almost 100% death after 30 min of incubation at peptide concentrations of 30 and 60 μM. Even at low peptide concentrations of 3 and 6 μM, only ~10% of the bacterial cells survived the incubation with PuroA. These two lowest peptide concentrations

Table 4
Dissociation constants (Kds) for the puroindoline derived peptides binding to pET-19b plasmid DNA and *E. coli* polar lipid extract LUVs. Error ranges are the standard deviation of three separate experiments.

Peptide	DNA Kd (μM)	Lipid Kd (μM)	Ratio lipid Kd:DNA Kd
PuroB1	53.0 ± 3.5	42.4 ± 2.9	0.8
PuroB2	9.6 ± 11.9	41.1 ± 6.1	4.3
PuroB3	3.1 ± 4.5	19.6 ± 3.6	6.4
PuroB4	20.7 ± 8.2	36.6 ± 11.1	1.8
PuroB5	2.3 ± 0.2	23.8 ± 6.0	10.4
PuroA	0.4 ± 0.2	1.0 ± 0.1	2.2

were tested in the macromolecular synthesis assay and it was found that PuroA blocked the incorporation of tritiated precursors of DNA, RNA and protein (Fig. 9). This effect was almost immediate as there was a distinct drop in the radioactive counts for samples taken after 5 min of incubation with the peptide.

The PuroB2, PuroB3 and PuroB5 peptides were also tested for their ability to inhibit macromolecular synthesis in *E. coli*. Over the course of 30 min incubation, PuroB2 did not kill a significant amount, even at a concentration as high as 60 μM (Fig. 9). In spite of the lack of killing, PuroB2 did block the incorporation of tritiated precursors into DNA, RNA and protein in a concentration dependent manner. Even at a sub-MIC concentration of 6 μM, PuroB2 caused a slight decrease in the amount of DNA, RNA and protein generated in the *E. coli* cultures. When the peptide concentration was increased to 30 and 60 μM, a more substantial decrease in the amount of DNA, RNA and protein was observed.

PuroB3 and PuroB5 both have MICs of ~6 μM against *E. coli* and they demonstrated similar abilities to inhibit macromolecular synthesis *in vivo* (Fig. 9). After 30 min of incubation with both peptides, less than 10% survival was observed at concentrations of 60 μM so this concentration was not tested in the macromolecular synthesis assays. At lower peptide concentrations, where a number of *E. coli* cells survived the 30 minute incubation, there was a substantial decrease in the amount of DNA, RNA and protein that was produced. Even at a peptide concentration of 3 μM, which is below the MIC, both PuroB3 and PuroB5 caused a decrease in the production of DNA, RNA and protein. At 30 μM, both PuroB3 and PuroB5 blocked the incorporation of tritiated thymidine, uridine and histidine into DNA, RNA and protein similar to the effects observed with the control antibiotics.

The macromolecular synthesis assays presented here demonstrate that the PuroB peptides are capable of blocking synthesis of DNA, RNA and protein in bacterial cells. This correlates with the observed

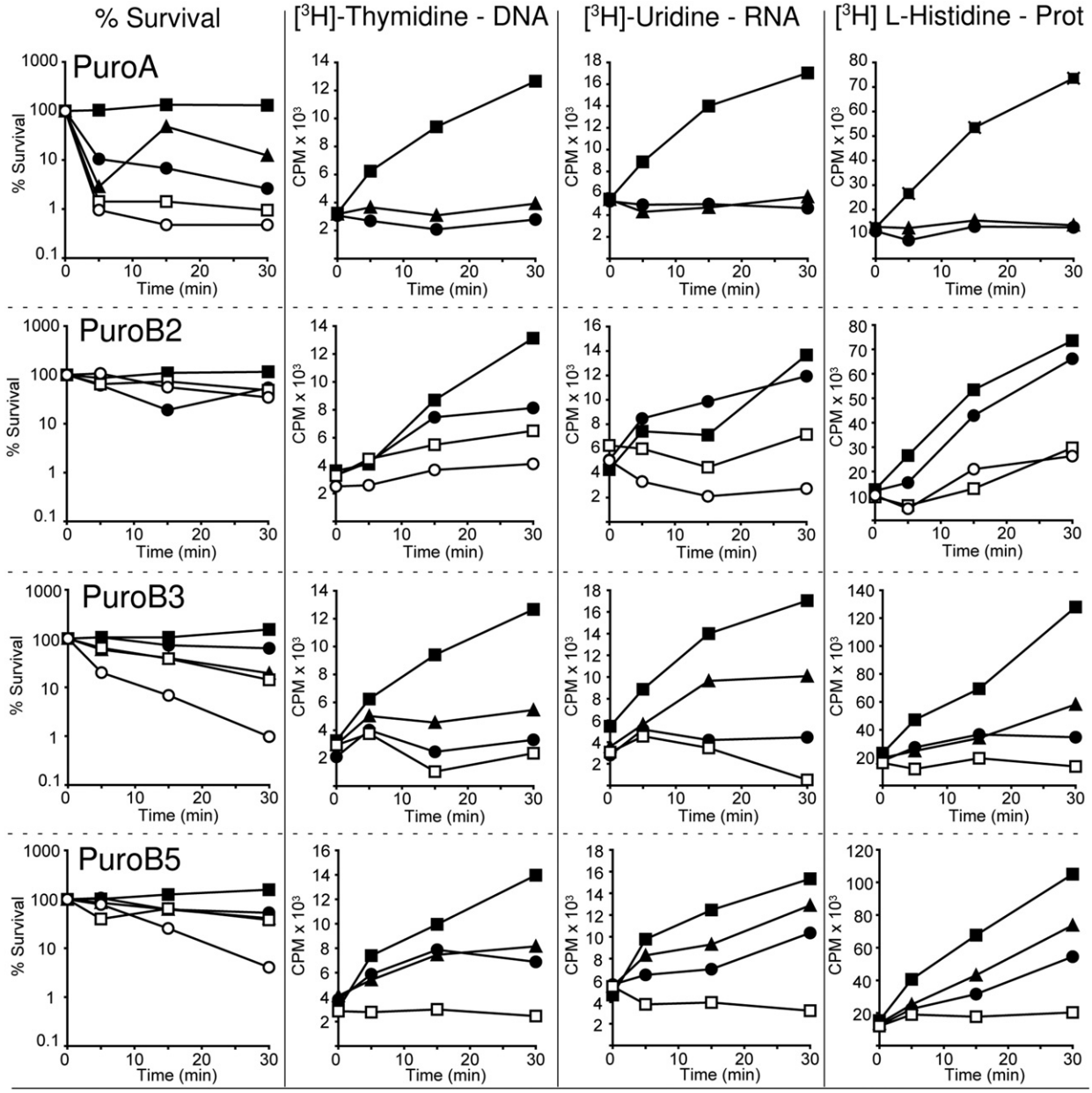

Fig. 9. Effect of the puroindoline peptides on bacterial survival and macromolecular synthesis in *E. coli* CGSC 4908. Bacterial survival in the presence of peptide was examined at peptide concentrations of 3(▲), 6(●), 30(□) and 60 μM(○). The effect of peptide on the incorporation of [^{3}H]-thymidine into DNA, [^{3}H]-uridine into RNA and [^{3}H]L-histidine into protein was also measured and compared to a control sample lacking peptide (■). Data are presented as radioactive counts per minute (CPM) and representative results from two separate trials are shown.

potency of the PuroB peptides and is likely related to the antibacterial mode of action.

4. Discussion

The mode of action of many antimicrobial peptides is usually attributed to the perturbation of the bacterial cytoplasmic membrane which directly leads to the release of cellular components and cell death [1]. Most of the biophysical studies presented here are consistent with the binding of the puroindoline B derived peptides to negatively charged membranes, which implicates lipid binding as a step in the mode of action of the PuroB peptides.

All the PuroB peptides were relatively unstructured in aqueous solution and only folded in the presence of detergent micelles, where they adopted a largely amphipathic turn-like structure (Fig. 6). Two antimicrobial peptides with similar amino acid composition to the puroindoline derived peptides are tritrpticin and indolicin. These antimicrobial peptides are also rich in Trp residues and exhibit a large net cationic charge [52]. Interestingly, both of these peptides adopt stable turn-like structures in the presence of detergent micelles [20,54] and it is possible that this is a feature of Trp-rich cationic antimicrobial peptides.

The emission fluorescence results suggest that the PuroB peptides interact at the interfacial region of a bilayer and that the Trp residues embed themselves into the hydrophobic core of the membrane. The DSC results demonstrated that the PuroB peptides selectively interact with anionic phospholipids but they also increase the T_{hex} in DiPoPE lipid suspensions. All of these results are consistent with a membrane active mode of action [49,52] that was previously proposed for the related PuroA peptide [21]. However, the calcein leakage and membrane depolarization assay clearly demonstrate that the PuroB peptides do not significantly disrupt the integrity of phospholipid bilayers to the same levels seen for other membrane active peptides. As a result, an alternative molecular target for the PuroB derived peptides was sought.

The idea of non-membrane targeting by antimicrobial peptides has been postulated for some time [55–57] and experimental evidence for intracellular targets continues to appear in the literature. Indirect evidence comes from confocal microscopy studies of fluorescently tagged peptides wherein the peptides cross the bacterial membrane and localize within the cytoplasm [5,58,59], suggesting that these peptides exert their antimicrobial effect intracellularly. Data supporting direct interactions between antimicrobial peptides and intracellular components is also available. For instance, buforin II, a highly potent antimicrobial peptide produced in the stomach tissue of the Asian toad *Bufo bufo garagriozans* [60], has higher antimicrobial activity than the well known lytic peptide, magainin 2, but it does not effectively permeabilize membranes [61]. Instead, Buforin II translocates across membranes without causing significant lipid flip-flop [61] and localizes to the cytoplasm of bacterial cells [43]. Buforin II is also known to interact with DNA and RNA [43], offering compelling evidence that this antimicrobial peptide acts intracellularly. It should be noted that buforin II is derived from histone H2A [60]. Histones are highly basic proteins responsible for DNA packing in eukaryotic nuclei and therefore, the ability of buforin II to interact with DNA may be an intrinsic trait of this sequence. However, non-histone derived antimicrobial peptides have also been shown to bind directly to DNA [62] and RNA [63] suggesting that this may be a general feature of a number of antimicrobial peptide sequences.

Recently, novel intracellular binding targets for antimicrobial peptides have been identified which implicate non-membrane mediated mechanisms of action as the primary cause of bacterial cell death. Examples include direct inhibition of DNA repair machinery within the bacterial cell [64] or interactions between antimicrobial peptides and ATP, which sequesters the high energy molecule from the activity of ATP-dependent enzymes [65]. Proteomics approaches have also been used to identify protein binding targets for antimicrobial peptides [66]. It is becoming increasingly apparent that intracellular targeting by antimicrobial peptides may be part of a complex combination of factors that all contribute to the antimicrobial mechanism of action.

The agarose gel retardation assays presented here reveal that the PuroB peptides are capable of binding plasmid DNA. Of particular interest is that the most potent antibacterial PuroB peptides, B2, B3 and B5, have the greatest affinity for the plasmid DNA. Additionally, the affinity of PuroB2, B3 and B5 for the plasmid DNA is stronger than the affinity of these peptides to lipids (Table 4), suggesting that these peptides would prefer to bind to DNA over phospholipids. These results correlate well with the observed antimicrobial activities of the PuroB peptides and it is attractive to propose a mechanism of antimicrobial activity wherein the puroindoline derived peptides spontaneously translocate into the cytoplasm of bacterial cells and bind to nucleic acids within the cell. Unfortunately, the agarose gel retardation assay is not direct evidence that these peptides block transcription and translation in vivo. PuroB2, B3 and B5 have the largest cationic charge of all the PuroB derivatives and it is possible that the positively charged peptides are interacting with the polyanionic DNA similar to the electrostatic attraction between the peptides and negatively charged membranes.

To establish a link between the DNA binding assay and the antimicrobial activity of the PuroB peptides, we performed macromolecular synthesis inhibition assays using radioactive precursors for DNA, RNA and protein biosynthesis and monitored isotope incorporation over time. Similar experiments have been applied to macromolecular synthesis studies of bacteria grown in the presence of bovine lactoferricin [67], indolicidin [68], lysozyme derived peptides [69] and pleurocidin derived peptides [44]. When tested at concentrations near the MIC, PuroB2, PuroB3 and PuroB5 caused a rapid and substantial decrease in the amount of radioactive precursor incorporated into DNA, RNA and protein. This demonstrates that the PuroB peptides inhibit the processes of transcribing the DNA strand into mRNA, the translation of the mRNA into protein and DNA replication itself.

Notably, PuroA also significantly inhibited macromolecular synthesis at sub-inhibitory concentrations of the peptide (Fig. 9). Previous experiments showed that PuroA significantly caused calcein leakage from POPC:POPG LUVs [21] but the current work indicates that this membrane disrupting property depends on the fluidity of the membrane and the degree of saturation in the acyl chains (see Fig. 7B). Additionally, PuroA does not appear to disrupt cytoplasmic membrane integrity in *E. coli* cells, suggesting that the antibacterial activity may be more complex than originally postulated. The interaction between PuroA and the bacterial membrane is probably an intermediate step in the mechanism of action of this peptide. PuroA likely initially interacts with the bacterial phospholipids followed by translocation into the bacterial cell, where it ultimately exerts its antibacterial effect.

It is possible that intracellular mechanisms of action have been overlooked in other antimicrobial peptide studies. If a peptide demonstrates significant pore forming or lytic properties, then one of the conventional membrane destabilizing models [1,49,52] is usually applied to explain the observed activity. However, in instances where a peptide does not cause significant membrane destabilization, only then are other binding targets sought to explain the mode of action. The results from the studies with the PuroA peptide clearly demonstrate that a strong membrane destabilizing effect does not necessarily preclude additional mechanisms, such as binding to intracellular DNA, RNA or proteins.

Predicting whether a peptide sequence will be predominantly membrane active or act intracellularly is not a trivial endeavor. Many studies into the biological effect of tritrpticins and indolicidins have focused on membrane interactions, implicating a membrane mode of action for these peptides [70–75]. However, our group has recently discovered that tritrpticin can bind to plasmid DNA (unpublished results) and there is significant evidence that indolicidin

acts intracellularly [62,68]. Even short Trp- and Arg-rich peptides derived from lysozyme cause minimal membrane perturbations [5] while causing rapid inhibition of macromolecular synthesis in *E. coli* [69]. This feature may not be limited to Trp-rich peptides with turn-like structures. For instance, magainin 2 is a peptide that adopts helical structure in the presence of micelles [76] but it has also been shown to enter bacterial cells [77] and has the ability to bind DNA and RNA [43], albeit with lower affinity compared to other peptides [78]. This observation further highlights the importance of comparing the strength of peptide binding to intracellular components compared to the affinity of the peptide to phospholipids.

The structural requirements for antimicrobial peptide binding to DNA have only recently been examined for a handful of peptides. A molecular dynamics simulation of buforin II bound to nucleic acids revealed that positively charged residues form strong interactions with the phosphate groups in the nucleic acid backbone [79]. Considering that the phosphodiester backbone is integral to DNA sequences, the authors hypothesized that buforin II targets DNA in a non-sequence specific manner [79]. The molecular dynamics simulations of buforin II also suggested that the peptide maintained a helical conformation when bound to DNA. However, a circular dichroism study revealed that buforin II actually adopts an extended conformation when bound to DNA [78]. In addition to buforin II, the structures of magainin 2 and pleurocidin bound to duplex DNA and membranes were also studied by CD spectroscopy. Interestingly, these two peptides more readily adopted α-helical conformations when bound to membranes compared to buforin II. However, the affinity of magainin 2 and pleurocidin for DNA was weaker than that seen with buforin II, leading the authors to conclude that peptide helicity is likely directly related to membrane activity but does not contribute to interactions with duplex DNA [78]. Evidently, more structural studies of antimicrobial peptide binding to DNA are required to fully understand the interactions that are occurring at the molecular level.

The results presented here for the puroindoline derived antimicrobial peptides reveal a mode of action that combines membrane interactions with intracellular targeting. Our current model for the mechanism of action involves the PuroB peptides partitioning into negatively charged membranes where they adopt a largely amphipathic structure with the Trp residues embedded into the hydrophobic core of the membrane. Interestingly, the PuroB peptides do not disrupt membranes to a large enough extent to allow for leakage of calcein from LUVs or extensive membrane depolarization. Instead, it appears that the PuroB peptides translocate across the bacterial membrane where they preferentially bind to nucleic acids within the cell and block the synthesis of DNA, RNA and proteins. Various mechanisms of peptide translocation have been proposed which do not involve disruption of the overall integrity of the bacterial cytoplasmic membrane [28,49] but the exact mechanism of PuroB membrane translocation remains to be elucidated.

The biophysical studies of the PuroB derivatives have significant implications for antimicrobial peptide research in general. Most studies reported to date have focused on understanding the interactions between antimicrobial peptides and membranes and thus far only limited attention has been devoted to intracellular targeting of antimicrobial peptides. Identifying novel targets for antimicrobial peptides and understanding their underlying molecular interactions are important aspects for future research into antimicrobial peptides. Eventually, the current efforts to enhance membrane interactions and translocation might one day be augmented by efforts to strengthen the molecular interactions between antimicrobial peptides and DNA, RNA or proteins. Ultimately, generating truly novel and potent antimicrobial sequences will require optimizing peptide sequences that efficiently pass through membranes and simultaneously bind strongly to intracellular components.

Acknowledgements

The authors would like to thank Dr. Deane McIntyre for his dedication and service to the NMR facility at the University of Calgary. Thanks also to Dr. Kasia Stevens for assistance with the radioactive assays and Dr. Leonard T. Nguyen and Mauricio Arias for helpful discussions. This work was supported by the Canadian Institutes of Health Research (CIHR) program for "Alternatives to Antibiotics" (HJV) and by the Natural Sciences and Engineering Research Council (NSERC) discovery grant 293595-07 (DGS). HJV is an Alberta Innovates–Health Solutions (AIHS) Scientist.

Appendix A. Supplementary data

Supplementary data to this article can be found online at http://dx.doi.org/10.1016/j.bbamem.2013.03.023.

References

[1] L.T. Nguyen, E.F. Haney, H.J. Vogel, The expanding scope of antimicrobial peptide structures and their modes of action, Trends Biotechnol. 29 (2011) 464–472.
[2] W. Bellamy, M. Takase, H. Wakabayashi, K. Kawase, M. Tomita, Antibacterial spectrum of lactoferricin-B, a potent bactericidal peptide derived from the N-terminal region of bovine lactoferrin, J. Appl. Bacteriol. 73 (1992) 472–479.
[3] J.L. Gifford, H.N. Hunter, H.J. Vogel, Lactoferricin: a lactoferrin-derived peptide with antimicrobial, antiviral, antitumor and immunological properties, Cell. Mol. Life Sci. 62 (2005) 2588–2598.
[4] M.I.A. van der Kraan, J. Groenink, K. Nazmi, E.C.I. Veerman, J.G.M. Bolscher, A.V.N. Amerongen, Lactoferrampin: a novel antimicrobial peptide in the N1-domain of bovine lactoferrin, Peptides 25 (2004) 177–183.
[5] H.N. Hunter, W. Jing, D.J. Schibli, T. Trinh, I.Y. Park, S.C. Kim, H.J. Vogel, The interactions of antimicrobial peptides derived from lysozyme with model membrane systems, Biochim. Biophys. Acta 1668 (2005) 175–189.
[6] H. Kawasaki, S. Iwamuro, Potential roles of histones in host defense as antimicrobial agents, Infect. Disord. Drug Targets 8 (2008) 195–205.
[7] H.S. Tsao, S.A. Spinella, A.T. Lee, D.E. Elmore, Design of novel histone-derived antimicrobial peptides, Peptides 30 (2009) 2168–2173.
[8] J.E. Blochet, C. Chevalier, E. Forest, E. Pebay-Peyroula, M.F. Gautier, P. Joudrier, M. Pezolet, D. Marion, Complete amino acid sequence of puroindoline, a new basic and cystine-rich protein with a unique tryptophan-rich domain, isolated from wheat endosperm by Triton X-114 phase partitioning, FEBS Lett. 329 (1993) 336–340.
[9] M.F. Gautier, M.E. Aleman, A. Guirao, D. Marion, P. Joudrier, *Triticum aestivum* puroindolines, two basic cystine-rich seed proteins: cDNA sequence analysis and developmental gene expression, Plant Mol. Biol. 25 (1994) 43–57.
[10] P. Charnet, G. Molle, D. Marion, M. Rousset, V. Lullien-Pellerin, Puroindolines form ion channels in biological membranes, Biophys. J. 84 (2003) 2416–2426.
[11] C.F. Morris, Puroindolines: the molecular genetic basis of wheat grain hardness, Plant Mol. Biol. 48 (2002) 633–647.
[12] A. Nadolska-Orczyk, S. Gasparis, W. Orczyk, The determinants of grain texture in cereals, J. Appl. Genet. 50 (2009) 185–197.
[13] L. Dubreil, T. Gaborit, B. Bouchet, D.J. Gallant, W.F. Broekaert, L. Quillien, D. Marion, Spatial and temporal distribution of the major isoforms of puroindolines (puroindoline-a and puroindoline-b) and non specific lipid transfer protein (ns-LTPle(1)) of *Triticumaestivum* seeds. Relationships with their in vitro antifungal properties, Plant Sci. 138 (1998) 121–135.
[14] D. Palumbo, M. Iannaccone, A. Porta, R. Capparelli, Experimental antibacterial therapy with puroindolines, lactoferrin and lysozyme in *Listeria monocytogenes* infected mice, Microbes Infect. 12 (2010) 538–545.
[15] X. Cheng, G. Liu, G. Ye, H. Wang, X. Shen, K. Wu, J. Xie, I. Altosaar, Screening and cloning of antimicrobial DNA sequences using a vital staining method, Gene 430 (2009) 132–139.
[16] R. Capparelli, I. Ventimiglia, D. Palumbo, D. Nicodemo, P. Salvatore, M.G. Amoroso, M. Iannaccone, Expression of recombinant puroindolines for the treatment of staphylococcal skin infections (acne vulgaris), J. Biotechnol. 128 (2007) 606–614.
[17] P. Llanos, M. Henriquez, J. Minic, K. Elmorjani, D. Marion, G. Riquelme, J. Molgo, E. Benoit, Puroindoline-a and alpha1-purothionin form ion channels in giant liposomes but exert different toxic actions on murine cells, FEBS J. 273 (2006) 1710–1722.
[18] M.E. Selsted, M.J. Novotny, W.L. Morris, Y.Q. Tang, W. Smith, J.S. Cullor, Indolicidin, a novel bactericidal tridecapeptide amide from neutrophils, J. Biol. Chem. 267 (1992) 4292–4295.
[19] C. Lawyer, S. Pai, M. Watabe, P. Borgia, T. Mashimo, L. Eagleton, K. Watabe, Antimicrobial activity of a 13 amino acid tryptophan-rich peptide derived from a putative porcine precursor protein of a novel family of antibacterial peptides, FEBS Lett. 390 (1996) 95–98.
[20] D.J. Schibli, P.M. Hwang, H.J. Vogel, Structure of the antimicrobial peptide tritrpticin bound to micelles: a distinct membrane-bound peptide fold, Biochemistry 38 (1999) 16749–16755.

[21] W. Jing, A.R. Demcoe, H.J. Vogel, Conformation of a bactericidal domain of puroindoline a: structure and mechanism of action of a 13-residue antimicrobial peptide, J. Bacteriol. 185 (2003) 4938–4947.
[22] E. Gasteiger, C. Hoogland, A. Gattiker, S. Duvaud, M.R. Wilkins, R.D. Appel, A. Bairoch, J.M. Walker, Protein identification and analysis tools on the ExPASy Server, The Proteomics Protocols Handbook, Humana Press, Totowa, NJ, 2005, pp. 571–601.
[23] I. Andre, S. Linse, Measurement of Ca2+-binding constants of proteins and presentation of the CaLigator software, Anal. Biochem. 305 (2002) 195–205.
[24] J.R. Lakowicz, Quenching of Fluorescence, Principles of Fluorescence Spectroscopy, vol. Second, Kluwer Academic, New York, NY, 1999, pp. 237–265.
[25] E.F. Haney, F. Lau, H.J. Vogel, Solution structures and model membrane interactions of lactoferrampin, an antimicrobial peptide derived from bovine lactoferrin, Biochim. Biophys. Acta 1768 (2007) 2355–2364.
[26] D.J. Schibli, R.F. Epand, H.J. Vogel, R.M. Epand, Tryptophan-rich antimicrobial peptides: comparative properties and membrane interactions, Biochem. Cell Biol. 80 (2002) 667–677.
[27] E.J. Prenner, R.N.A.H. Lewis, L.H. Kondejewski, R.S. Hodges, R.N. McElhaney, Differential scanning calorimetric study of the effect of the antimicrobial peptide gramicidin S on the thermotropic phase behavior of phosphatidylcholine, phosphatidylethanolamine and phosphatidylglycerol lipid bilayer membranes, Biochim. Biophys. Acta 1417 (1999) 211–223.
[28] J.P.S. Powers, A. Tan, A. Ramamoorthy, R.E.W. Hancock, Solution structure and interaction of the antimicrobial polyphemusins with lipid membranes, Biochemistry 44 (2005) 15504–15513.
[29] B.A. Wallace, R.W. Janes, An Introduction to Circular Dichroism and Synchrotron Radiation Circular Dichroism Spectroscopy, in: P.I. Haris (Ed.), Modern Techniques for Circular Dichroism and Synchrotron Radiation Circular Dichroism Spectroscopy, IOS Press, Amsterdam, 2009, pp. 1–18.
[30] T.L. Hwang, A.J. Shaka, Water suppression that works — excitation sculpting using arbitrary wave-forms and pulsed-field gradients, J. Magn. Reson. A 112 (1995) 275–279.
[31] F. Delaglio, S. Grzesiek, G.W. Vuister, G. Zhu, J. Pfeifer, A. Bax, Nmrpipe — a multidimensional spectral processing system based on unix pipes, J. Biomol. NMR 6 (1995) 277–293.
[32] B.A. Johnson, Using NMRView to visualize and analyze the NMR spectra of macromolecules, Methods Mol. Biol. 278 (2004) 313–352.
[33] A.T. Brunger, P.D. Adams, G.M. Clore, W.L. Delano, P. Gros, R.W. Grosse-Kunstleve, J.S. Jiang, J. Kuszewski, M. Nilges, N.S. Pannu, R.J. Read, L.M. Rice, T. Simonson, G.L. Warren, Crystallography & NMR system: A new software suite for macromolecular structure determination, Acta Crystallogr. D: Biol. Crystallogr. 54 (1998) 905–921.
[34] J.P. Linge, S.I. O'Donoghue, M. Nilges, Automated assignment of ambiguous nuclear overhauser effects with ARIA, Methods Enzymol. 339 (2001) 71–90.
[35] G.N. Ramachandran, C. Ramakrishnan, V. Sasisekharan, Stereochemistry of polypeptide chain configurations, J. Mol. Biol. 7 (1963) 95–99.
[36] R. Koradi, M. Billeter, K. Wuthrich, MOLMOL: a program for display and analysis of macromolecular structures, J. Mol. Graph. 14 (1996) 51–55.
[37] R.A. Laskowski, J.A.C. Rullmann, M.W. MacArthur, R. Kaptein, J.M. Thornton, AQUA and PROCHECK-NMR: Programs for checking the quality of protein structures solved by NMR, J. Biomol. NMR 8 (1996) 477–486.
[38] L.T. Nguyen, D.J. Schibli, H.J. Vogel, Structural studies and model membrane interactions of two peptides derived from bovine lactoferricin, J. Pept. Sci. 11 (2005) 379–389.
[39] B.N. Ames, E.F. Neufeld, V. Ginsberg, Assay of inorganic phosphate, total phosphate and phosphatases, Meth. Enzymol, Academic Press, New York, 1966, pp. 115–118.
[40] N.P. Chongsiriwatana, A.E. Barron, Comparing bacterial membrane interactions of antimicrobial peptides and their mimics, Methods Mol. Biol. 618 (2010) 171–182.
[41] M.H. Richmond, D.C. Clark, S. Wotton, Indirect method for assessing the penetration of beta-lactamase-nonsusceptible penicillins and cephalosporins in *Escherichia coli* strains, Antimicrob. Agents Chemother. 10 (1976) 215–218.
[42] M. Wu, E. Maier, R. Benz, R.E.W. Hancock, Mechanism of interaction of different classes of cationic antimicrobial peptides with planar bilayers and with the cytoplasmic membrane of *Escherichia coli*, Biochemistry 38 (1999) 7235–7242.
[43] C.B. Park, H.S. Kim, S.C. Kim, Mechanism of action of the antimicrobial peptide buforin II: buforin II kills microorganisms by penetrating the cell membrane and inhibiting cellular functions, Biochem. Biophys. Res. Commun. 244 (1998) 253–257.
[44] A. Patrzykat, C.L. Friedrich, L. Zhang, V. Mendoza, R.E.W. Hancock, Sublethal concentrations of pleurocidin-derived antimicrobial peptides inhibit macromolecular synthesis in *Escherichia coli*, Antimicrob. Agents Chemother. 46 (2002) 605–614.
[45] T. Maniatis, Molecular Cloning: a Laboratory Manual, vol. 1st, Cold Spring Harbour Laboratory, 1982, p. 68.
[46] K. Lohner, The role of membrane lipid composition in cell targeting of antimicrobial peptides, Development of Novel Antimicrobial Agents: Emerging Strategies, Horizon Scientific Press, Norfolk, England, 2001, pp. 149–165.
[47] K.J. Hallock, D.K. Lee, A. Ramamoorthy, MSI-78, an analogue of the magainin antimicrobial peptides, disrupts lipid bilayer structure *via* positive curvature strain, Biophys. J. 84 (2003) 3052–3060.
[48] P.E. Smith, J.R. Brender, A. Ramamoorthy, Induction of negative curvature as a mechanism of cell toxicity by amyloidogenic peptides: the case of islet amyloid polypeptide, J. Am. Chem. Soc. 131 (2009) 4470–4478.
[49] E.F. Haney, S. Nathoo, H.J. Vogel, E.J. Prenner, Induction of non-lamellar lipid phases by antimicrobial peptides: a potential link to mode of action, Chem. Phys. Lipids 163 (2010) 82–93.
[50] I.B. Grishina, R.W. Woody, Contributions of tryptophan side chains to the circular dichroism of globular proteins: exciton couplets and coupled oscillators, Faraday Discuss. 99 (1994) 245–262.
[51] S.M. Kelly, T.J. Jess, N.C. Price, How to study proteins by circular dichroism, Biochim. Biophys. Acta 1751 (2005) 119–139.
[52] D.I. Chan, E.J. Prenner, H.J. Vogel, Tryptophan- and arginine-rich antimicrobial peptides: structures and mechanisms of action, Biochim. Biophys. Acta 1758 (2006) 1184–1202.
[53] S.S. Cohen, M. Sekiguchi, J.L. Stern, H.D. Barner, The synthesis of messenger RNA without protein synthesis in normal and phage-infected thymineless strains of *Escherichia coli*, Proc. Natl. Acad. Sci. U. S. A. 49 (1963) 699–707.
[54] A. Rozek, C.L. Friedrich, R.E.W. Hancock, Structure of the bovine antimicrobial peptide indolicidin bound to dodecylphosphocholine and sodium dodecyl sulfate micelles, Biochemistry 39 (2000) 15765–15774.
[55] L. Otvos Jr., Antibacterial peptides and proteins with multiple cellular targets, J. Pept. Sci. 11 (2005) 697–706.
[56] J.D. Hale, R.E.W. Hancock, Alternative mechanisms of action of cationic antimicrobial peptides on bacteria, Expert Rev. Anti Infect. Ther. 5 (2007) 951–959.
[57] M. Cudic, L. Otvos Jr., Intracellular targets of antibacterial peptides, Curr. Drug Targets 3 (2002) 101–106.
[58] J.P. Powers, M.M. Martin, D.L. Goosney, R.E.W. Hancock, The antimicrobial peptide polyphemusin localizes to the cytoplasm of Escherichia coli following treatment, Antimicrob. Agents Chemother. 50 (2006) 1522–1524.
[59] A.J. Rezansoff, H.N. Hunter, W. Jing, I.Y. Park, S.C. Kim, H.J. Vogel, Interactions of the antimicrobial peptide Ac-FRWWHR-NH(2) with model membrane systems and bacterial cells, J. Pept. Res. 65 (2005) 491–501.
[60] C.B. Park, M.S. Kim, S.C. Kim, Novel antimicrobial peptide from Bufo bufo gargarizans, Biochem. Biophys. Res. Commun. 218 (1996) 408–413.
[61] S. Kobayashi, K. Takeshima, C.B. Park, S.C. Kim, K. Matsuzaki, Interactions of the novel antimicrobial peptide buforin 2 with lipid bilayers: proline as a translocation promoting factor, Biochemistry 39 (2000) 8648–8654.
[62] C.H. Hsu, C. Chen, M.L. Jou, A.Y. Lee, Y.C. Lin, Y.P. Yu, W.T. Huang, S.H. Wu, Structural and DNA-binding studies on the bovine antimicrobial peptide, indolicidin: evidence for multiple conformations involved in binding to membranes and DNA, Nucleic Acids Res. 33 (2005) 4053–4064.
[63] S.C. Park, J.Y. Kim, C. Jeong, S. Yoo, K.S. Hahm, Y. Park, A plausible mode of action of pseudin-2, an antimicrobial peptide from *Pseudis paradoxa*, Biochim. Biophys. Acta 1808 (2011) 171–182.
[64] L.Y. Su, D.L. Willner, A.M. Segall, An antimicrobial peptide that targets DNA repair intermediates *in vitro* inhibits Salmonella growth within murine macrophages, Antimicrob. Agents Chemother. 54 (2010) 1888–1899.
[65] K. Hilpert, B. McLeod, J. Yu, M.R. Elliott, M. Rautenbach, S. Ruden, J. Burck, C. Muhle-Goll, A.S. Ulrich, S. Keller, R.E.W. Hancock, Short cationic antimicrobial peptides interact with ATP, Antimicrob. Agents Chemother. 54 (2010) 4480–4483.
[66] Y.H. Tu, Y.H. Ho, Y.C. Chuang, P.C. Chen, C.S. Chen, Identification of lactoferricin B intracellular targets using an *Escherichia coli* proteome chip, PLoS One 6 (2011) e28197.
[67] H. Ulvatne, O. Samuelsen, H.H. Haukland, M. Kramer, L.H. Vorland, Lactoferricin B inhibits bacterial macromolecular synthesis in *Escherichia coli* and *Bacillus subtilis*, FEMS Microbiol. Lett. 237 (2004) 377–384.
[68] C. Subbalakshmi, N. Sitaram, Mechanism of antimicrobial action of indolicidin, FEMS Microbiol. Lett. 160 (1998) 91–96.
[69] A. Pellegrini, U. Thomas, P. Wild, E. Schraner, R. von Fellenberg, Effect of lysozyme or modified lysozyme fragments on DNA and RNA synthesis and membrane permeability of *Escherichia coli*, Microbiol. Res. 155 (2000) 69–77.
[70] V.V. Andrushchenko, H.J. Vogel, E.J. Prenner, Interactions of tryptophan-rich cathelicidin antimicrobial peptides with model membranes studied by differential scanning calorimetry, Biochim. Biophys. Acta 1768 (2007) 2447–2458.
[71] V.V. Andrushchenko, M.H. Aarabi, L.T. Nguyen, E.J. Prenner, H.J. Vogel, Thermodynamics of the interactions of tryptophan-rich cathelicidin antimicrobial peptides with model and natural membranes, Biochim. Biophys. Acta 1778 (2008) 1004–1014.
[72] D.J. Schibli, L.T. Nguyen, S.D. Kernaghan, O. Rekdal, H.J. Vogel, Structure–function analysis of tritrpticin analogs: potential relationships between antimicrobial activities, model membrane interactions, and their micelle-bound NMR structures, Biophys. J. 91 (2006) 4413–4426.
[73] A.G. Vegh, K. Nagy, Z. Balint, A. Kerenyi, G. Rakhely, G. Varo, Z. Szegletes, Effect of antimicrobial peptide-amide: indolicidin on biological membranes, J. Biomed. Biotechnol. 2011 (2011) 670589.
[74] J.E. Shaw, J.R. Alattia, J.E. Verity, G.G. Prive, C.M. Yip, Mechanisms of antimicrobial peptide action: studies of indolicidin assembly at model membrane interfaces by in situ atomic force microscopy, J. Struct. Biol. 154 (2006) 42–58.
[75] J.C. Hsu, C.M. Yip, Molecular dynamics simulations of indolicidin association with model lipid bilayers, Biophys. J. 92 (2007) L100–L102.
[76] J. Gesell, M. Zasloff, S.J. Opella, Two-dimensional H-1 NMR experiments show that the 23-residue magainin antibiotic peptide is an alpha-helix in dodecylphosphocholine micelles, sodium dodecylsulfate micelles, and trifluoroethanol/water solution, J. Biomol. NMR 9 (1997) 127–135.
[77] H.H. Haukland, H. Ulvatne, K. Sandvik, L.H. Vorland, The antimicrobial peptides lactoferricin B and magainin 2 cross over the bacterial cytoplasmic membrane and reside in the cytoplasm, FEBS Lett. 508 (2001) 389–393.
[78] Y. Lan, Y. Ye, J. Kozlowska, J.K. Lam, A.F. Drake, A.J. Mason, Structural contributions to the intracellular targeting strategies of antimicrobial peptides, Biochim. Biophys. Acta 1798 (2010) 1934–1943.
[79] E.T. Uyterhoeven, C.H. Butler, D. Ko, D.E. Elmore, Investigating the nucleic acid interactions and antimicrobial mechanism of buforin II, FEBS Lett. 582 (2008) 1715–1718.